

LARGE-SCALE DYNAMOS AT LOW MAGNETIC PRANDTL NUMBERS

AXEL BRANDENBURG

NORDITA, AlbaNova University Center, Roslagstullsbacken 23, SE-10691 Stockholm, Sweden; brandenb@nordita.org

Received 2008 August 6; accepted 2009 March 13; published 2009 May 11

ABSTRACT

Using direct simulations of hydromagnetic turbulence driven by random polarized waves it is shown that dynamo action is possible over a wide range of magnetic Prandtl numbers from 10^{-3} to 1. Triply periodic boundary conditions are being used. In the final saturated state the resulting magnetic field has a large-scale component of Beltrami type. For the kinematic phase, growth rates have been determined for magnetic Prandtl numbers between 0.01 and 1, but only the case with the smallest magnetic Prandtl number shows large-scale magnetic fields. It is less organized than in the nonlinear stage. For small magnetic Prandtl numbers the growth rates are comparable to those calculated from an alpha squared mean-field dynamo. In the linear regime the magnetic helicity spectrum has a short inertial range compatible with a $-5/3$ power law, while in the nonlinear regime it is the current helicity whose spectrum may be compatible with such a law. In the saturated case, the spectral magnetic energy in the inertial range is in slight excess over the spectral kinetic energy, although for small magnetic Prandtl numbers the magnetic energy spectrum reaches its resistive cut off wavenumber more quickly. The viscous energy dissipation declines with the square root of the magnetic Prandtl number, which implies that most of the energy is dissipated via Joule heat.

Key words: MHD – turbulence

Online-only material: color figures

1. INTRODUCTION

Many astrophysical plasmas are turbulent and tend to be magnetized. The magnetic fields can have typical length scales that are either larger or smaller than that of the energy-carrying eddies. We speak then correspondingly of large-scale or small-scale dynamos. Small-scale dynamos can already work in statistically mirror-symmetric isotropic homogeneous turbulence, whereas large-scale dynamos require in general a departure from parity-invariant or mirror-symmetric flows. The excitation conditions of small-scale dynamos depend sensitively on the value of the magnetic Prandtl number, i.e., the ratio of kinematic viscosity to magnetic diffusivity, $\text{Pr}_M = \nu/\eta$, where ν is the kinematic viscosity and η the magnetic diffusivity. This sensitivity is related to the fact that in the *kinematic* regime the spectral magnetic energy is peaked at the resistive scale. As was pointed out originally by Rogachevskii & Kleorin (1997), and more recently by Boldyrev & Cattaneo (2004), the slope of the kinetic energy spectrum is important for the onset of small-scale dynamo action. It matters therefore whether the resistive scale lies in the viscous range ($\text{Pr}_M \approx 1$), within the inertial range ($\text{Pr}_M \lesssim 0.1$), or right within the range where the bottleneck occurs ($\text{Pr}_M \approx 0.1$). The bottleneck effect refers to the spectral subrange just before the dissipation range where the kinetic energy spectrum is shallower than in the inertial range. Within the bottleneck range the velocity increments diverge even more strongly with decreasing separation than in the inertial range, making dynamo action harder still. Indeed, for small values of Pr_M the critical value of the magnetic Reynolds number above which small-scale dynamo action occurs increases therefore sharply toward $\text{Pr}_M = 0.1$ (Schekochihin et al. 2005), and then decreases slightly for $\text{Pr}_M < 0.05$ (Iskakov et al. 2007). However, even with the computing power available today, direct simulations of small-scale dynamo action are still only marginally possible at such small values of Pr_M .

For certain types of flows dynamo action is easier to achieve even though Pr_M is small. The Taylor–Green flow is an example

where the critical value of the magnetic Reynolds number becomes constant for $\text{Pr}_M < 0.1$ (Ponty et al. 2004, 2005). In this flow there can be large-scale patches with finite kinetic helicity of opposite sign. A completely different example is fully helical turbulence where the excitation condition for dynamo action is virtually unchanged as Pr_M decreases from 1 to 0.1 (Brandenburg 2001, hereafter B01). For an ABC-flow dynamo, Mininni (2007) found a weak dependence of the threshold value of the magnetic Reynolds number Re_M on Pr_M . For $\text{Pr}_M < 0.1$ the threshold value seemed to become asymptotically independent of Pr_M and dynamo action was demonstrated for values of Pr_M down to 5×10^{-3} .

In many astrophysical bodies, Pr_M is indeed rather small (around 10^{-5}). Such systems still possess dynamo action and can have large-scale magnetic fields. It is likely that such systems belong to the second class of systems where the excitation conditions are not drastically altered toward small values of Pr_M . Indeed, large-scale magnetic fields are found regardless of whether Pr_M is small (e.g., the Sun and other stars with outer convection zones, as well as planets) or large (e.g., in spiral galaxies, because of their low densities).

The purpose of this paper is to point out that a strong Pr_M dependence does not occur in systems where the magnetic field generation is predominantly due to a large-scale dynamo. Such systems have been studied in idealized settings such as periodic boxes using explicit forcing functions for driving the turbulence. This has significant advantages in that periodic boundary conditions can be used, energy spectra are easily computed and, most importantly, isotropy and homogeneity eases comparison with turbulence theory. A disadvantage is that the magnetic helicity can only change on resistive timescales, which slows down the saturation (B01).

With these provisions in mind, we consider now simulations of maximally helical turbulence in triply periodic boxes where we keep in most cases the fluid Reynolds number, $\text{Re} = u_{\text{rms}}/\nu k_f$, constant and vary the magnetic Reynolds number, $\text{Re}_M = u_{\text{rms}}/\eta k_f$, and thereby $\text{Pr}_M (\equiv \text{Re}_M/\text{Re})$. Here, u_{rms}

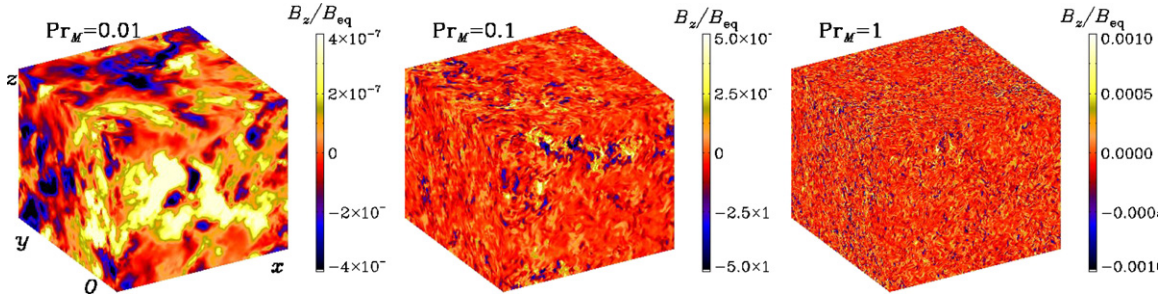


Figure 1. Visualization of B_z for $\text{Pr}_M = 0.01, 0.1,$ and 1 at $\text{Re} = 670$. Note the emergence of a large-scale pattern for $\text{Pr}_M = 0.01$. For $\text{Pr}_M = 0.1$ there are only a few extended patches and for $\text{Pr}_M = 1$ the field is completely random and of small scale only. The orientation of the axes is indicated for the first panel, and is the same for all other panels.

(A color version of this figure is available in the online journal.)

is the rms velocity of the turbulence and k_f is the forcing wavenumber. According to B01 the dynamo should be excited whenever the domain is large enough (2–3 times larger than the forcing scale) and the magnetic Reynolds number exceeds unity ($\text{Re}_M \geq 1.1 \dots 1.4$ or so). This was confirmed for magnetic Prandtl numbers as low as 0.1. In the present work we consider kinematic dynamo action down to values of $\text{Pr}_M = 10^{-2}$ and nonlinear saturated dynamos down to $\text{Pr}_M = 10^{-3}$.

2. THE METHOD

We solve the hydromagnetic equations for velocity \mathbf{U} , logarithmic density $\ln \rho$, and magnetic vector potential \mathbf{A} for an isothermal gas in the presence of an externally imposed helical forcing function \mathbf{f} ,

$$\frac{\partial \mathbf{U}}{\partial t} = -\mathbf{U} \cdot \nabla \mathbf{U} - c_s^2 \nabla \ln \rho + \mathbf{f} + \rho^{-1} (\mathbf{J} \times \mathbf{B} + \nabla \cdot 2\rho \nu \mathbf{S}) \quad (1)$$

$$\frac{\partial \ln \rho}{\partial t} = -\mathbf{U} \cdot \nabla \ln \rho - \nabla \cdot \mathbf{U} \quad (2)$$

$$\frac{\partial \mathbf{A}}{\partial t} = \mathbf{U} \times \mathbf{B} - \mu_0 \eta \mathbf{J}. \quad (3)$$

Here, $\mathbf{B} = \nabla \times \mathbf{A}$ is the magnetic field, $\mathbf{J} = \nabla \times \mathbf{B} / \mu_0$ is the current density, μ_0 is the vacuum permeability, c_s is the isothermal speed of sound, and $\mathbf{S}_{ij} = \frac{1}{2}(U_{i,j} + U_{j,i}) - \frac{1}{3}\delta_{ij} \nabla \cdot \mathbf{U}$ is the traceless rate of strain tensor. We consider a triply periodic domain of size L^3 , so the smallest wavenumber in the domain is $k_1 = 2\pi/L$. The forcing function consists of eigenfunctions of the curl operator with positive eigenvalues and is therefore fully helical with $\mathbf{f} \cdot \nabla \times \mathbf{f} = k \mathbf{f}^2$, where $3.5 \leq k/k_1 \leq 4.5$ is wavenumber interval of the forcing function, whose average value is referred to as $k_f = 4k_1$. The amplitude of \mathbf{f} is such that the Mach number is $u_{\text{rms}}/c_s \approx 0.1$, so compressive effects are negligible (Dobler et al. 2003).

The initial conditions consist of a weak Beltrami field. The initial velocity is zero and the initial density is uniform with $\rho = \rho_0 = \text{const}$. Note that the volume-averaged density remains constant, i.e., $\langle \rho \rangle = \rho_0$.

The model is equivalent to that of B01, except that there the value of k_f/k_1 was chosen to be either 5 or 30. In order for large-scale dynamo action to be possible, k_f/k_1 must at least be larger than 2 (Haugen et al. 2004), but 3 is already sufficient (Brandenburg et al. 2008). In the kinematic regime the fastest growing mode is expected to have the wavenumber $k_f/2$, so in order that this wavenumber is distinct from k_1 , we have chosen $k_f/k_1 = 4$ throughout this paper.

3. RESULTS

We begin by presenting results for $\text{Re} \approx 670$ where we vary Pr_M in the range $0.01 \leq \text{Pr}_M \leq 1$, i.e., Re_M is varied in the range $6.7 \leq \text{Re}_M \leq 670$. The dynamo is excited in all those cases, but the growth rate λ varies. We consider first the kinematic regime where the magnetic field is weak and turn then to the nonlinear regime where the magnetic field has saturated. Most of the results presented below have been obtained at a resolution of 512^3 meshpoints. The solution was first evolved at lower resolution (128^3 meshpoints), then remeshed to twice the resolution, again evolved for some time, and finally remeshed to 512^3 meshpoints, and again evolved for some time. Data for the kinematic regime are only used after the initial transients have disappeared and a clear exponential growth has developed at all length scales for at least some 40 turnover times (also for the runs with a resolution of 512^3 meshpoints). The run with 128^3 meshpoints has been evolved all the way into saturation, and it was then remeshed twice by a factor of 2, just like in the kinematic regime.

3.1. Field Structure in the Kinematic Regime

Visualizations of one component of the magnetic field show the emergence of a large-scale magnetic field for small values of Pr_M . This is clearly demonstrated in Figure 1, where we see for $\text{Pr}_M = 0.01$ a large-scale pattern with a systematic variation in the y direction. For $\text{Pr}_M = 0.1$ there is no such variation, although there are some extended patches in which the field orientation is the same. For $\text{Pr}_M = 1$ even this is no longer the case and the field appears completely random with small-scale variations only.

We emphasize that random and patch-like structures only occur in the kinematic regime. In the saturated regime a large-scale field emerges in all cases. This will be discussed in Section 3.7.

3.2. Growth Rates

The growth rate is calculated as the average of the instantaneous growth rate, $d \ln B_{\text{rms}}/dt$. Examples are shown in Figure 2 for runs with $\text{Re} = 670$ and different values of Pr_M using 512^3 meshpoints. In Figure 3, we show growth rates normalized by $u_{\text{rms}} k_f$ (inverse turnover times) as a function of Re_M for three values of Re_M and compare with the corresponding results for nonhelical turbulence forced at larger scales in the wavenumber interval $1 \leq k/k_1 \leq 2$ (Haugen et al. 2004). In that case we use $k_f = 1.5$ for the average value. The small-scale dynamo is then only excited when $\text{Re}_M \geq 35$. For $\text{Re}_M \geq 100$ the growth rates

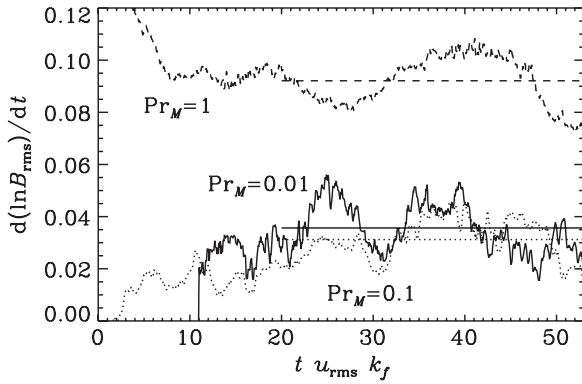


Figure 2. Instantaneous growth rate for runs with different values of Pr_M and 512^3 meshpoints. The straight lines give the growth rates obtained by averaging over the indicated time interval. The solid, dotted, and dashed lines are for $\text{Pr}_M = 0.01, 0.1,$ and $1,$ respectively.

for helical turbulence with $k_f = 4$ are quite similar to those of nonhelical turbulence with $k_f = 1.5$. We have also calculated growth rates for the nonhelical case with $k_f = 4$ and find the same values as in the helical case. We note that in all cases, and even for small values of Pr_M , the growth rates based on the rms magnetic field are equal to those based on the rms values of the mean fields obtained by averaging over any two coordinate directions.

In both helical and nonhelical cases, when Re_M is large enough, λ increases like $\text{Re}_M^{1/2}$, as expected (Schekochihin et al. 2004). This is because the eddy turnover rate at the resistive scale is $\propto k_\eta^{2/3}$, but because $k_\eta/k_f \propto \text{Re}_M^{3/4}$ we have $\lambda \propto \text{Re}_M^{1/2}$. However, when there is also large-scale dynamo action, one expects there to be a lower bound for λ given by the growth rate for the large-scale dynamo, λ_{LS} . Using the theory for an α^2 dynamo (Moffatt 1978, Krause & Rädler 1980), we have

$$\lambda_{\text{LS}} = |\alpha k| - (\eta + \eta_t)k^2, \quad (4)$$

where α is a pseudo scalar (the α effect) and η_t is the turbulent magnetic diffusivity. For fully helical turbulence we have $|\alpha| \approx u_{\text{rms}}/3$ and $\eta_t \approx u_{\text{rms}}/3k_f$ (Sur et al. 2008), so we can write the growth rate as

$$\frac{\lambda_{\text{LS}}}{u_{\text{rms}}k_f} = \frac{1}{3} \frac{k_1}{k_f} \left[1 - \frac{k_1}{k_f} (1 + 3\text{Re}_M^{-1}) \right], \quad (5)$$

where we have put $|k| = k_1$. Over the parameter range considered in this paper ($\text{Re}_M \geq 6.7$ and $k_f/k_1 = 4$), $\lambda_{\text{LS}}/u_{\text{rms}}k_f$ increases only slightly from 0.053 to 0.062 as Re_M increases.

The result shown in Figure 3 gives values that are systematically below λ_{LS} . There could be two reasons for this discrepancy. On the one hand, the accuracy of the estimates $|\alpha| \approx u_{\text{rms}}/3$ and $\eta_t \approx u_{\text{rms}}/3k_f$ may not be good enough. On the other hand, Equation (4) is only an approximation in cases where $\lambda_{\text{LS}} \neq 0$, because then memory effects become important. This means that, when allowing α and η_t to be integral kernels in time, they are no longer proportional to δ functions, but have finite widths in time. This effect has recently been studied by Hubbard & Brandenburg (2008) and can be quite dramatic in some cases.

In Figure 3, we have varied Re_M by changing Pr_M and keeping $\text{Re} = \text{const} = 670$. We can therefore also consider this graph as a representation of the magnetic Prandtl number dependence of λ . However, Pr_M can also be changed while keeping $\text{Re}_M = \text{const} = 6.7$. The corresponding result is shown

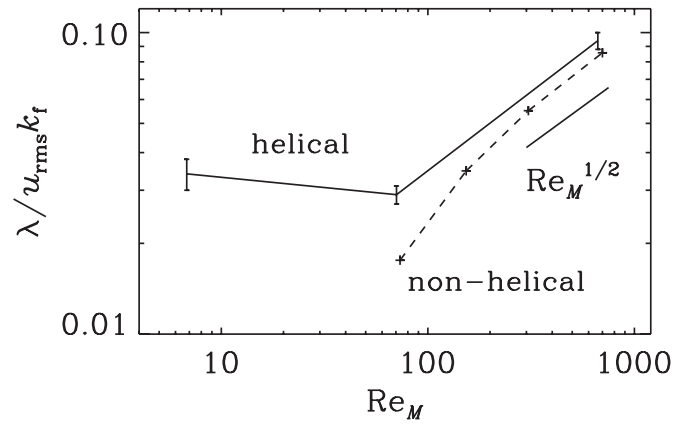


Figure 3. Dynamo growth rates of the rms magnetic field for helical turbulence with $\text{Re} = 670$ (solid line) compared with growth rates for nonhelical turbulence (dashed lines; adapted from Haugen et al. 2004).

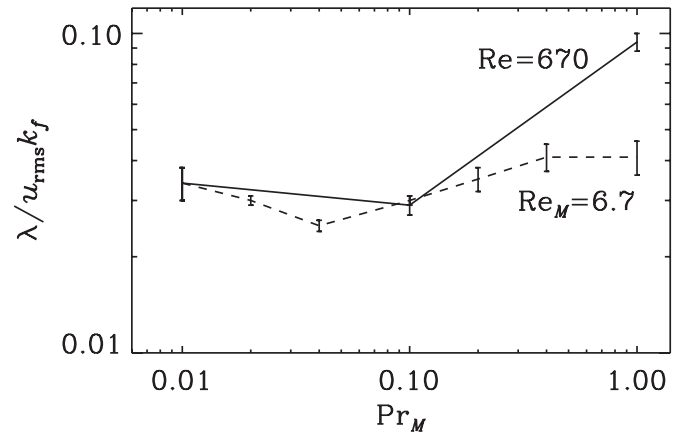


Figure 4. Dependence of dynamo growth rates of the rms magnetic field on Pr_M for helical turbulence with $\text{Re}_M = 6.7$ (dashed line) and $\text{Re} = 670$ (solid line). Here the solid line corresponds to the solid line in Figure 3.

in Figure 4 and compared with the previous case. The two graphs are in reasonable agreement for small values of Pr_M , but the rise of λ for $\text{Re} = 670$ around $\text{Pr}_M = 1$ is not seen in the case with $\text{Re}_M = 6.7$. This suggests that the transition from a purely large-scale turbulent dynamo to a mixed large-scale and small-scale turbulent dynamo requires values of Re_M above some critical value (somewhere between 10 and 100), and is not just determined by the value of Pr_M .

3.3. Spectra

The transition from a purely large-scale turbulent dynamo to a mixed large-scale and small-scale turbulent dynamo is accompanied by characteristic changes in the spectral properties of the magnetic field. In the following we employ shell-integrated spectra of kinetic and magnetic energy, $E(k)$ and $M(k)$, respectively, as well as of kinetic and magnetic helicities, $F(k)$ and $H(k)$, respectively. These spectra are normalized such that $\int E(k) dk = \frac{1}{2} \langle U^2 \rangle \equiv E$, $\int M(k) dk = \frac{1}{2} \langle B^2 \rangle \equiv M$, $\int F(k) dk = \langle \mathbf{W} \cdot \mathbf{U} \rangle$, and $\int H(k) dk = \langle \mathbf{A} \cdot \mathbf{B} \rangle$, where $\mathbf{W} = \nabla \times \mathbf{U}$ is the vorticity.

In Figure 5, we plot $E(k)$ and $M(k)$ for three cases with $\text{Pr}_M = 1, 0.1,$ and 0.01 , keeping $\text{Re} = 670$ in all cases. The magnetic energy spectra are compensated by $\exp(-\lambda t)$, where λ is the numerically determined growth rate for each run, and then averaged in time. We consider here only the kinematic regime when the magnetic energy is weak. The kinetic energy

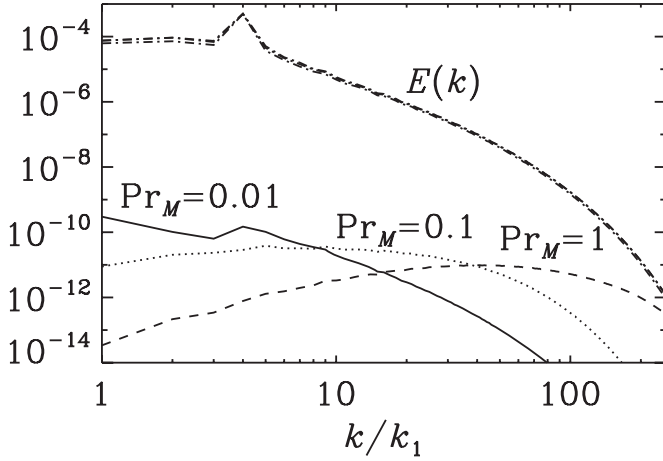


Figure 5. Spectra of kinetic and magnetic energies in the kinematic regime for $Pr_M = 0.01, 0.1, \text{ and } 1$.

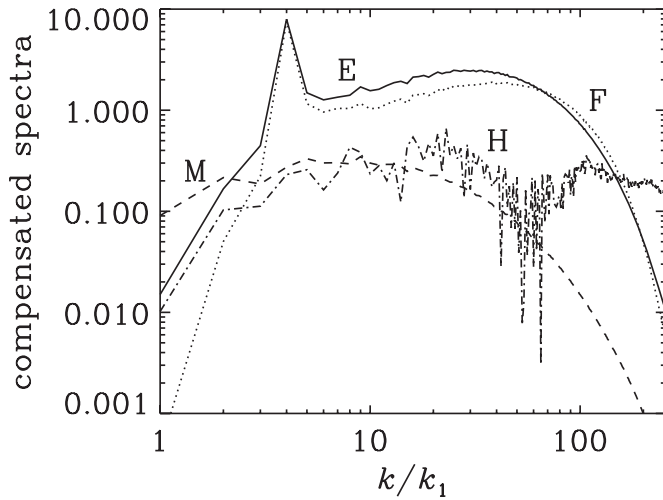


Figure 6. Compensated spectra of kinetic and magnetic energies and helicities in the kinematic regime for $Pr_M = 1$. The spectra are denoted by letters E, F, M, and H, as described in the text.

spectra are then always the same. Since the magnetic energy is weak, we have scaled the magnetic energy spectra for different Pr_M to an arbitrarily chosen reference value of 10^{-6} below the kinetic energy spectrum. For $Pr_M = 1$ the magnetic energy seems to follow an approximate Kazantsev (1968) spectrum with a range proportional to $k^{3/2}$ and is peaked at the resistive scale near $k/k_1 = 50$. For smaller values of Pr_M the peak of magnetic energy moves to smaller wavenumbers.

In order to judge the correspondence with various power-law scalings we label, in Figure 6, various compensated spectra as follows:

$$\text{label E: } E(k) \epsilon_K^{-2/3} k^{5/3}, \quad (6)$$

$$\text{label F: } |F(k)| \epsilon_K^{-2/3} k^{5/3} / 2k_f, \quad (7)$$

$$\text{label M: } M(k) k_f (k/k_*)^{-3/2} / M, \quad (8)$$

$$\text{label H: } |H(k)| k_f \epsilon_K^{-2/3} k^{5/3} E / 2M, \quad (9)$$

where $k_* = \int k M(k) dk / M$ is the wavenumber where the magnetic energy spectrum peaks and ϵ_K is the kinetic energy dissipation per unit mass. The compensated kinetic energy

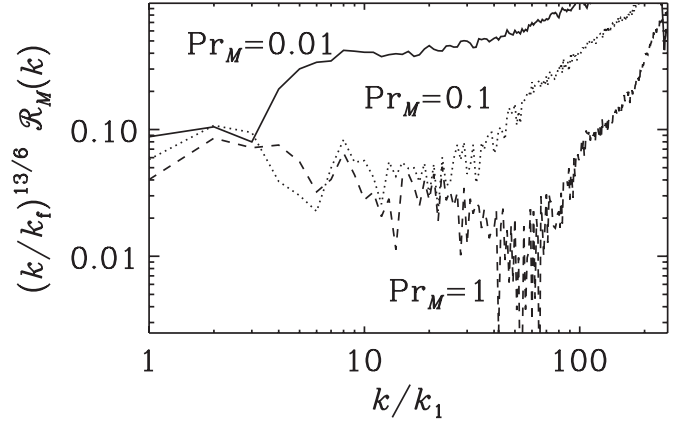


Figure 7. Relative spectral magnetic helicity, $k|H(k)|/2M(k)$, compensated by $(k/k_f)^{13/6}$, for Pr_M ranging from 0.01 to 1.

spectrum shows a bottleneck that is clearly stronger than in the case without helicity (e.g., Kaneda et al. 2003, Haugen & Brandenburg 2006). The kinetic helicity spectrum shows a similar spectrum that also has a strong bottleneck, which is particularly evident when it is compensated by $k^{5/3}$. The existence of a $k^{5/3}$ subrange for the modulus of the kinetic helicity spectrum is well known from early closure calculations (André & Lesieur 1977), and has also been seen in direct numerical simulations (Borue & Orszag 1997; Brandenburg & Subramanian 2005a) and in shell model calculations (Ditlevsen & Giuliani 2001). Such a scaling implies that the relative spectral kinetic helicity,

$$\mathcal{R}_K(k) \equiv F(k)/2kE(k), \quad (10)$$

decreases toward small scales like k^{-1} and has a maximum at $k = k_f$ with $\mathcal{R}_K(k_f) = 0.96$. At that scale, the relative magnetic helicity,

$$\mathcal{R}_M(k) \equiv kH(k)/2M(k), \quad (11)$$

is $-0.15, -0.08, \text{ and } +0.42$ for $Pr_M = 1, 0.1, \text{ and } 0.01$, respectively. The realizability condition implies that the moduli of $\mathcal{R}_K(k)$ and $\mathcal{R}_M(k)$ are less than unity (Moffatt 1969). The positive sign for $Pr_M = 0.01$ agrees with the idea that the helical driving of the flow imprints a helical field of the same sense at the same scale. Owing to an inverse cascade of magnetic helicity (Pouquet et al. 1976), $H(k)$ is of opposite sign at large scales. While this is very clearly established in the nonlinear regime (B01) or for small values of Pr_M , a larger range of scales attains negative values during the linear stage when $Pr_M = 0.1$ and 1.

For the magnetic helicity we also find an approximate $|H(k)| \sim k^{-5/3}$ spectrum, which is different from the nonlinear case when the current helicity, $C(k) = k^2 H(k)$ shows a $k^{-5/3}$ spectrum (Brandenburg & Subramanian 2005a). Assuming that $M(k) \sim k^{3/2}$, the relative spectral helicity would seem to decrease now more rapidly like $k|H(k)|/2M(k) \sim k^{-13/6}$. Figure 7 shows that the correspondingly compensated magnetic helicity to energy ratio changes now less strongly in the range $4 \leq k/k_1 \leq 40$.

3.4. Saturation Regime

Eventually the initial exponential growth comes to a halt and is followed by a resistively long saturation phase during which a large-scale magnetic field develops at wavenumber k_1 , regardless of the value of k_f . Owing to the use of periodic

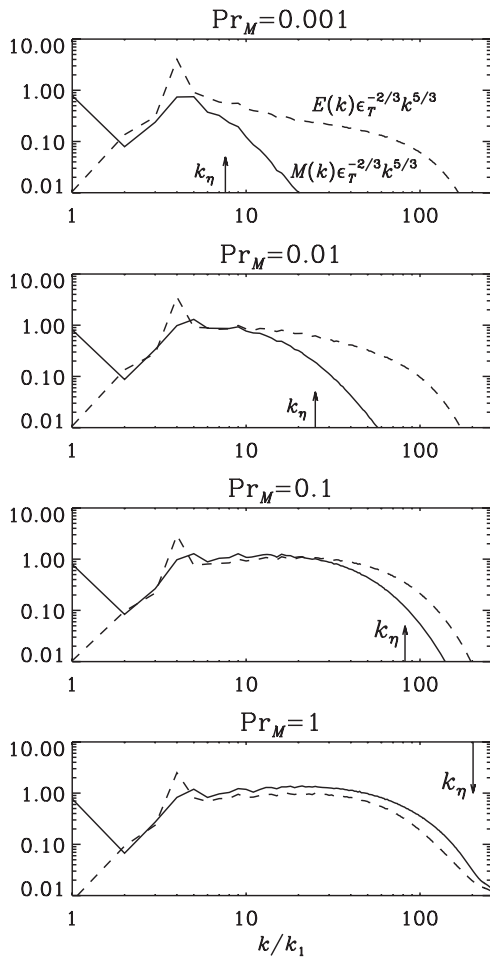


Figure 8. Kinetic and magnetic energy spectra in the saturated regime for $\text{Pr}_M = 10^{-3}$ with $\text{Re} = 4400$, $\text{Pr}_M = 10^{-2}$ with $\text{Re} = 2300$, $\text{Pr}_M = 0.1$ with $\text{Re} = 1200$, and $\text{Pr}_M = 1$ with $\text{Re} = 450$. All spectra are compensated by $\epsilon_T^{-2/3} k^{5/3}$. The ohmic dissipation wavenumber, $k_\eta = (\epsilon_M/\eta^3)^{1/4}$, is indicated by an arrow. The viscous dissipation wavenumbers are 430, 350, 290, and 180 for $\text{Pr}_M = 10^{-3}$, 10^{-2} , 0.1, and 1, respectively.

boundary conditions, this large-scale field tends to be force-free and fully helical, and its energy per unit volume is by a factor $k_f/k_1 = 4$ larger than the value at k_f , which in turn is comparable to the kinetic energy per unit volume. For details see B01. Here we only consider the end of this slow saturation phase. Compensated kinetic and magnetic energy spectra are shown in Figure 8 for magnetic Prandtl numbers ranging from 1 to down to 10^{-3} .

In the final saturated state, and especially for $\text{Pr}_M = 1$, the $M(k)$ and $E(k)$ spectra are nearly on top of each other with $M(k)$ being slightly larger than $E(k)$ by 20%, which is qualitatively similar to the nonhelical case (cf. Haugen et al. 2003). There are indications of a somewhat shallower spectrum due to a bottleneck effect both for kinetic and magnetic energies just before the two enter the viscous and resistive dissipation ranges. Also for $\text{Pr}_M = 0.1$ there is a short range where $M(k)$ exceeds $E(k)$, but then, not surprisingly, $M(k)$ turns into the dissipation range before $E(k)$ does. This is even more clearly the case for $\text{Pr}_M = 0.01$.

Low- Pr_M turbulence has the interesting property that for given numerical resolution much larger fluid Reynolds numbers can be achieved than for $\text{Pr}_M = 1$. This is simply because almost all the energy is dissipated resistively, and the energy that continues along the kinetic energy cascade is comparatively weak, so not

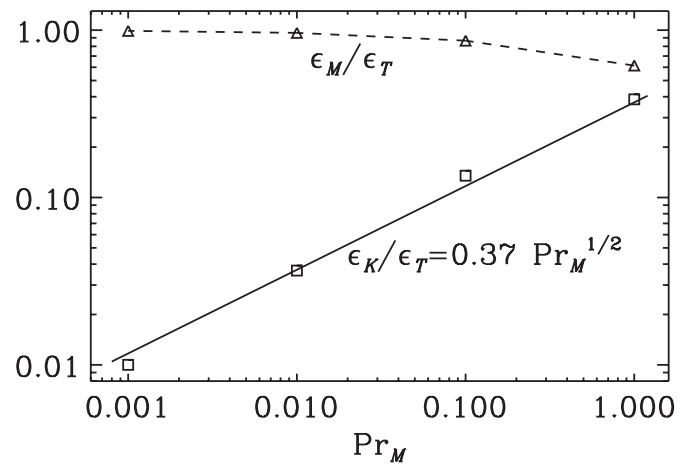


Figure 9. Dependence of the fractional kinetic and magnetic energy dissipation rates. Note that the fractional kinetic energy dissipation decreases with decreasing Pr_M to the $1/2$ power.

much viscosity is needed for dissipating the remaining kinetic energy. In fact, for $\text{Pr}_M = 0.01$ we were able to go to $\text{Re} = 2300$ with a resolution of only 512^3 meshpoints. For $\text{Pr}_M = 0.1$ and 1 and the same resolution we could only go to $\text{Re} = 1200$ and 450, respectively.

3.5. Diverting Most of the Energy into Joule Heat

As has recently been stressed by Mininni (2007), an increasing fraction of energy is being dissipated via Joule dissipation, as Pr_M decreases. In Figure 9, we plot the dependence of the kinetic and magnetic energy dissipation rates per unit mass, $\epsilon_K = \langle 2\rho v \mathbf{S}^2 \rangle / \rho_0$ and $\epsilon_M = \langle \eta \mu_0 \mathbf{J}^2 \rangle / \rho_0$, relative to the total dissipation, $\epsilon_T = \epsilon_K + \epsilon_M$, versus Pr_M . The data are well described by a power-law fit of the form

$$\epsilon_K/\epsilon_T \approx 0.37 \text{Pr}_M^{1/2}. \quad (12)$$

Thus, for $\text{Pr}_M = 1$ about the 37% of the energy is dissipated into viscous heat, while 63% is dissipated via Joule dissipation. This is similar to the case of nonhelical hydromagnetic turbulence (Haugen et al. 2003), where these numbers are about 30% and 70%, respectively.

In turbulence the energy dissipation is generally proportional to U^3/L , where U is the typical velocity and L is a typical length scale. Conventionally one defines a dimensionless dissipation parameter as

$$C_\epsilon = \frac{\epsilon_T}{U^3/L}, \quad (13)$$

where U is the one-dimensional rms velocity, which is related to u_{rms} via $U^2 = u_{\text{rms}}^2/3$, and L is the integral scale and is related to k_f via $\frac{3}{4}\pi/k_f$. In nonhelical turbulence this value is typically around 0.5 (see also Pearson et al. 2004), but this value has never been determined for hydromagnetic turbulence with helicity. An exception is the work of Blackman & Field (2008), who considered a range of power-law scalings for kinetic and magnetic energy spectra to calculate analytically the dissipation rates.

It turns out that for our runs, $C_\epsilon \approx 1.5$, i.e. ≈ 3 times larger than the usual value; see Figure 10. Let us now discuss possible reasons for this difference. In the definition of the quantity C_ϵ one assumes that the energy flux scales with U^3/L . However, U is based on the typical rms velocity. In the presence of a strong

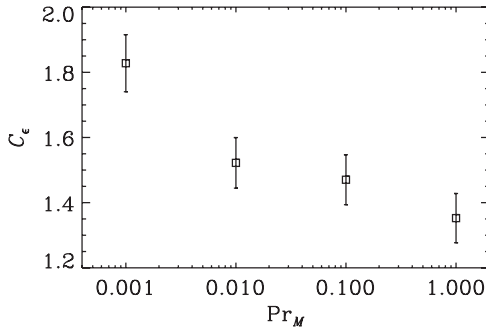


Figure 10. Dimensionless total energy dissipation rate, C_ϵ , as a function of Pr_M . Error bars have been estimated based on averages taken over each third of the full time series.

dynamo-generated magnetic field it may be sensible to base it on a combination of typical velocity and magnetic field strength. In our case we have $\langle \mathbf{B}^2 / \mu_0 \rangle / \langle \rho \mathbf{U}^2 \rangle \approx 2$, so U would need to be scaled up by a factor $\sqrt{3}$, which reduces C_ϵ by a factor $3^{3/2} \approx 5$ to about 0.3. This value is nearly independent of the value of Pr_M , which was also found by Blackman & Field (2008) under plausible assumptions.

3.6. Helicity Spectra

As mentioned before, in the nonlinear regime both kinetic and current helicities, $F(k)$ and $C(k) = k^2 H(k)$, respectively, are expected to display a forward cascade with a $k^{-5/3}$ spectrum. If this is true, we would expect that within some wavenumber interval $|\mathcal{R}_K(k)|$ and $|\mathcal{R}_M(k)|$ decrease with increasing k like k^{-1} . In Figure 11 we show the correspondingly compensated relative kinetic and magnetic helicity spectra. It turns out that they are surprisingly similar regardless of the value of Pr_M . For $\text{Pr}_M = 1$ and 0.1 the compensated profiles of $\mathcal{R}_M(k)$ and $\mathcal{R}_K(k)$ are reasonably flat in the range $6 \leq k/k_1 \leq 14$. However, for $\text{Pr}_M = 10^{-2}$ and 10^{-3} the compensated profiles show an increase proportional to $k^{1/2}$. The fact that the anticipated k^{-1} scaling occurs only for magnetic Prandtl numbers down to 0.1 and only over an extremely short range may indicate that our Reynolds numbers are still too small to yield conclusive results. Especially at smaller scales, and certainly in the runs with the smallest Pr_M , the compensated relative kinetic and magnetic helicity spectra are compatible with a $k^{1/2}$ slope. This would imply a $k^{-7/6}$ spectrum for the kinetic and current helicities, which is shallower than that anticipated for a forward cascade, but still steeper than that in the case of equipartition. We emphasize again that this applies to the resistively controlled regime.

In Figure 11 we see that at $k = k_f$ both \mathcal{R}_K and \mathcal{R}_M are close to unity. This indicates that velocity and magnetic fields are nearly fully helical. However, for $k > k_f$ the velocity and magnetic fields become less helical, because the compensated relative helicities in Figure 11 increase with k not faster than to the $1/2$ power. On the other hand, for $k = k_1$ the magnetic field is again fully helical, i.e. $(k_1/k_f)|\mathcal{R}_M(k_1)|$ is equal to $k_1/k_f = 1/4$, but its helicity has the opposite sign.

In Table 1 we compare the values of $\mathcal{R}_M(k)$ during the linear and nonlinear stages at the wavenumbers k_1 and k_f for the three or four values of Pr_M . Note that during the nonlinear stage $\mathcal{R}_M(k_1)$ and $\mathcal{R}_M(k_f)$ are of opposite sign. The former is close to -1 while the latter increases from 0.52 to 0.72 as Pr_M decreases. As already indicated in Section 3.3, during the linear stage, the two are of opposite sign only for $\text{Pr}_M = 0.01$, while for larger

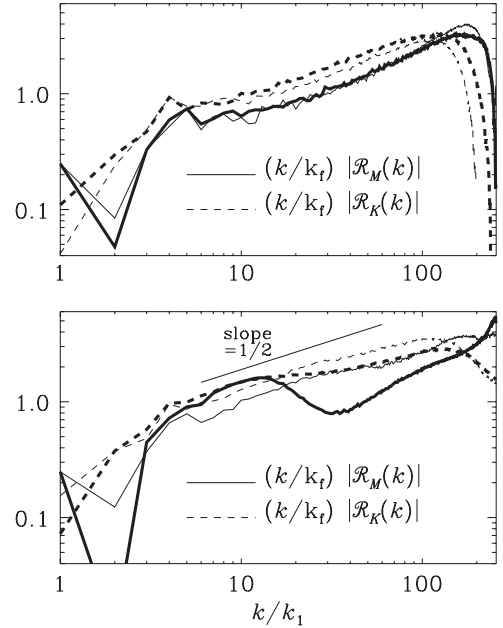


Figure 11. Spectral current and kinetic helicity ratios for the same four runs shown in Figure 8. The upper panel is for $\text{Pr}_M = 1$ (thin line) and 0.1 (thick line), while the lower panel is for 10^{-2} (thin line) and 10^{-3} (thick line). Note that for $\text{Pr}_M = 1$ and 0.1 the profiles of $(k/k_f)|\mathcal{R}_M(k)|$ and $(k/k_f)|\mathcal{R}_K(k)|$ are reasonably flat in the range $6 \leq k/k_1 \leq 14$. The $1/2$ slope is shown for comparison.

Table 1

Comparison of $\mathcal{R}_M(k_1)$ and $\mathcal{R}_M(k_f)$ During the Linear and Nonlinear Stages for Different Values of Pr_M

Pr_M	Linear		Nonlinear	
	k_1	k_f	k_1	k_f
10^{-3}			-0.993	+0.72
10^{-2}	-0.88	+0.42	-0.994	+0.66
10^{-1}	-0.59	-0.08	-0.993	+0.59
1	-0.41	-0.15	-0.993	+0.52

values of Pr_M a larger range of scales appears to be affected by the inverse transfer of magnetic helicity causing $\mathcal{R}_M(k_f)$ to be negative. It would be tempting to try and model this behavior using, for example, the four-scale helical dynamo model of Blackman (2003).

3.7. Effects on the Velocity Pattern

In Figure 12 we compare visualizations of B_z and U_z for all four values of Pr_M . The velocity and magnetic field patterns are surprisingly similar for all four values of Pr_M . Only for $\text{Pr}_M = 10^{-2}$ and 10^{-3} the magnetic field appears noticeably smoother than in the other two cases. The velocity field shows a marked anisotropy with small-scale elongated patterns aligned with the local direction of the mean magnetic field, which is here of the form $\overline{\mathbf{B}} \sim (0, \sin k_1 x, -\cos k_1 x)$. The anisotropy in the velocity can still be seen for small values of Pr_M , but the small-scale patterns are slightly smoother.

4. CONCLUSIONS

In many astrophysical bodies the magnetic Prandtl number is small, while in most simulations its value is chosen to be close to unity. As we have shown here, this mismatch is of relatively minor consequence for large-scale dynamos that are driven by helical forcing.

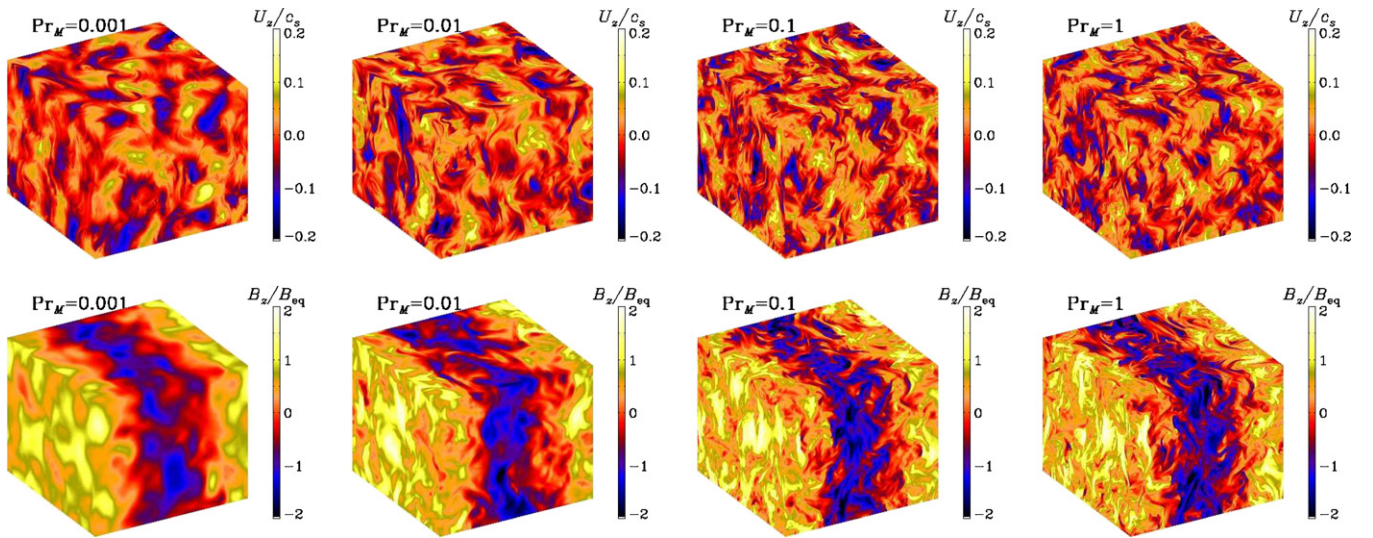


Figure 12. Visualizations of B_z and U_z for $\text{Pr}_M = 10^{-3}$ at $\text{Re} = 4400$ (left), $\text{Pr}_M = 10^{-2}$ at $\text{Re} = 2300$, $\text{Pr}_M = 0.1$ at $\text{Re} = 1200$, and $\text{Pr}_M = 1$ at $\text{Re} = 450$ (right). The orientation of the axes is the same as in Figure 1.

(A color version of this figure is available in the online journal.)

In the nonlinear stage, the velocity and magnetic field patterns are remarkably independent of the value of Pr_M . The only thing that changes is the length of the inertial range. A small magnetic Prandtl number simply means that the magnetic energy spectrum turns into the dissipation range more quickly than the kinetic energy spectrum. It also means that essentially all the energy is dissipated via Joule heat. This was recently also demonstrated by Mininni (2007). One reason is that the case of fully helical turbulence studied in the present paper is a particularly simple one, because it leads to uniform mean-field dynamo action with large-scale pattern formation covering the entire domain. In this paper we have seen that, at least for values of Re up to 4400, the dynamics of this large-scale pattern, i.e., of the large-scale magnetic field, is quite independent of how long the inertial range of the turbulence is. In the absence of helicity, there is only small-scale dynamo action, which is driven by the dynamics at the smallest possible scale, i.e. the resistive scale. In that case it does matter what the dynamics of the turbulence is at that scale. However, in that case it has not yet been possible to find dynamo action for values of Pr_M down to the values considered here. Nevertheless, it is possible that even in that case there is an asymptotic regime for large enough values of Re_M where the dynamics of the magnetic field is independent of the value of Pr_M , even though this regime is not yet accessible with present day computers.

To estimate the value of the magnetic Prandtl number in dense astrophysical bodies, one has to use the *Spitzer* formulae for η and ν . The resulting magnetic Prandtl number is (e.g., Brandenburg & Subramanian 2005b)

$$\text{Pr}_M = 1.1 \times 10^{-4} \left(\frac{T}{10^6 \text{ K}} \right)^4 \left(\frac{\rho}{0.1 \text{ g cm}^{-3}} \right)^{-1} \left(\frac{\ln \Lambda}{20} \right)^{-2}, \quad (14)$$

so at the bottom of the solar convection zone the magnetic Prandtl number is clearly rather small ($\sim 10^{-4}$). Nevertheless, simulations of solar and stellar dynamos available so far Pr_M are set to values of the order or unity. Although we have shown here that the resulting large-scale fields are similar to the more realistic case of small values of Pr_M , an important difference is that the small-scale dynamo may be more pronounced when

Pr_M is of order unity. In practice this means that a positive detection of dynamo action in a simulation might not necessarily be relevant for understanding the Sun, unless suitable conditions for the excitation of large-scale dynamo action are also met. On the other hand, once the large-scale dynamo is really excited, and if it is fully saturated, it is then quite feasible to lower the value of Pr_M significantly—without losing the large-scale dynamo. In fact, lowering Pr_M in a saturated large-scale dynamo means that most of the energy will be dissipated via Joule heating, and that the kinetic energy cascade only carries a small fraction of the total energy. This allows us to increase the value of Re , and hence to decrease the viscosity and thereby the value of Pr_M even further. Simulations of large-scale dynamo action in turbulent convection (Käpylä et al. 2008) provide one example where it is indeed feasible to lower Pr_M , although in that case the system is not uniform and so energy dissipation via Joule heating is only possible in those locations where the dynamo is strong enough (P. J. Käpylä 2008, private communication).

I thank Eric G. Blackman and Pablo Mininni for useful comments on the paper, and an anonymous referee for spotting a number of errors in the original version. It is a pleasure to acknowledge the organizers of the KITP program on dynamo theory and the staff of the KITP for providing a stimulating atmosphere. This research was supported in part by the National Science Foundation under grant PHY05-51164 and the Swedish Research Council under grant 621-2007-4064. The computations have been carried out at the National Supercomputer Centre in Linköping and at the Center for Parallel Computers at the Royal Institute of Technology in Sweden.

REFERENCES

- André, J.-C., & Lesieur, M. 1977, *J. Fluid Mech.*, **81**, 187
 Borue, V., & Orszag, S. A. 1997, *Phys. Rev. E*, **55**, 7005
 Blackman, E. G. 2003, *MNRAS*, **344**, 707
 Blackman, E. G., & Field, G. B. 2008, *MNRAS*, **386**, 1481
 Boldyrev, S., & Cattaneo, F. 2004, *Phys. Rev. Lett.*, **92**, 144501
 Brandenburg, A. 2001, *ApJ*, **550**, 824
 Brandenburg, A., Rädler, K.-H., Rheinhardt, M., & Subramanian, K. 2008, *ApJ*, **687**, L49
 Brandenburg, A., & Subramanian, K. 2005a, *A&A*, **439**, 835

- Brandenburg, A., & Subramanian, K. 2005b, *Phys. Rep.*, **417**, 1
- Ditlevsen, P. D., & Giuliani, P. 2001, *Phys. Rev. E*, **63**, 036304
- Dobler, W., Haugen, N. E. L., Yousef, T. A., & Brandenburg, A. 2003, *Phys. Rev. E*, **68**, 026304
- Haugen, N. E. L., & Brandenburg, A. 2006, *Phys. Fluids*, **18**, 075106
- Haugen, N. E. L., Brandenburg, A., & Dobler, W. 2003, *ApJ*, **597**, L141
- Haugen, N. E. L., Brandenburg, A., & Dobler, W. 2004, *Phys. Rev. E*, **70**, 016308
- Hubbard, A., & Brandenburg, A. 2008, *ApJ*, submitted, arXiv:0811.2561
- Iskakov, A. B., Schekochihin, A. A., Cowley, S. C., McWilliams, J. C., & Proctor, M. R. E. 2007, *Phys. Rev. Lett.*, **98**, 208501
- Kaneda, Y., Ishihara, T., Yokokawa, M., Itakura, K., & Uno, A. 2003, *Phys. Fluids*, **15**, L21
- Käpylä, P. J., Korpi, M. J., & Brandenburg, A. 2008, *A&A*, **491**, 353
- Kazantsev, A. P. 1968, *Sov. Phys.—JETP*, **26**, 1031
- Krause, F., & Rädler, K.-H. 1980, *Mean-field Magnetohydrodynamics and Dynamo Theory* (Oxford: Pergamon)
- Mininni, P. D. 2007, *Phys. Rev. E*, **76**, 026316
- Moffatt, H. K. 1969, *J. Fluid Mech.*, **35**, 117
- Moffatt, H. K. 1978, *Magnetic Field Generation in Electrically Conducting Fluids* (Cambridge: Cambridge Univ. Press)
- Pearson, B. R., Yousef, T. A., Haugen, N. E. L., Brandenburg, A., & Krogstad, P. Å. 2004, *Phys. Rev. E*, **70**, 056301
- Ponty, Y., Mininni, P. D., Montgomery, D. C., Pinton, J.-F., Politano, H., & Pouquet, A. 2005, *Phys. Rev. Lett.*, **94**, 164502
- Ponty, Y., Politano, H., & Pinton, J.-F. 2004, *Phys. Rev. Lett.*, **92**, 144503
- Pouquet, A., Frisch, U., & Léorat, J. 1976, *J. Fluid Mech.*, **77**, 321
- Rogachevskii, I., & Kleeorin, N. 1997, *Phys. Rev. E*, **56**, 417
- Schekochihin, A. A., Cowley, S. C., Taylor, S. F., Maron, J. L., & McWilliams, J. C. 2004, *ApJ*, **612**, 276
- Schekochihin, A. A., Haugen, N. E. L., Brandenburg, A., Cowley, S. C., Maron, J. L., & McWilliams, J. C. 2005, *ApJ*, **625**, L115
- Sur, S., Brandenburg, A., & Subramanian, K. 2008, *MNRAS*, **385**, L15